Characterization of the 2007 Noto Hanto, Japan, earthquake

Haruo Horikawa

Active Fault Research Center, National Institute of Advanced Industrial Science and Technology (AIST), Tsukuba, Ibaraki 305-8567, Japan

(Received July 2, 2007; Revised November 27, 2007; Accepted December 5, 2007; Online published November 7, 2008)

Characterization of the 2007 Noto Hanto, Japan, earthquake (M_S 6.9), a moderate-size crustal event, was performed. The rupture process was firstly inferred from strong motion data. Inversion analysis revealed that the overall rupture finished within 6 s, and the seismic moment of this earthquake was estimated to be 1.1×10^{19} N m (M_w 6.6). Two areas of large slip and stress drop (asperities) were inferred on the fault plane. The maximum static stress drop calculated from the derived slip distribution exceeded 16 MPa for the major asperity, and the minor asperity has a similar maximum value. An area of negative stress drop corresponding to the distribution of small slip exists between the two asperities. This strongly suggests that the fault is segmented. A boundary between surface faults was located above the major asperity, but an area of negative stress drop appeared between the asperity and fault boundary. This suggests that the configuration of the surface faults reflects only a shallow part of the causative fault. The ratio of radiated energy to seismic moment was also estimated for the purpose of estimation of fault activity. Comparison of the derived value with those of other Japanese earthquakes suggests that the causative fault of the Noto Hanto earthquake is not very active.

Key words: 2007 Noto Hanto earthquake, rupture process, fault model, strong motion data, static stress change.

1. Introduction

The 2007 Noto Hanto earthquake (M_S 6.9), a moderate-size crustal event, occurred in the Noto region, located in the northernmost part of central Japan (Fig. 1). There are no historical documents that illustrate the occurrence of earthquakes greater than seven in the Noto region (Usami, 2003), and the seismicity of this region is not high. Consequently, little seismological attention has been paid to the region, and its seismic potential is poorly understood.

Surface faults are believed to be useful for the estimation of seismic potential. Katagawa *et al*. (2005) conducted a dense seismic survey in the west off-Noto area and have mapped three high-angle reverse fault systems associated with tiled blocks near the source region. Each fault system consists of two or three faults of about 10 km long. As discussed later in this report, two northeast-southwest aligned faults, which belong to one of the mapped fault systems, are likely to correspond to the causative fault. However, the northeastern extent of the northeastern surface fault is not clear due to limited seismic profiling near the coastal regions. On the other hand, no active fault in the peninsula has been found to the northeast of the surface fault (Ota *et al*., 1976). This detailed mapping provides a good opportunity to investigate the correspondence between surface faults and faults in depth. In this sense, characterization of the 2007 Noto Hanto earthquake is meaningful.

Repeat times of earthquakes are an important issue in evaluation of seismic potential. Trench excavation surveys have been extensively conducted for the purpose, but these have not been always successful. Coseismic behavior may provide a hint of this issue. In fact, the ratio of radiated energy to seismic moment is correlated with slip rate or repeat times of faults (Kanamori, 1994).

In this paper, I try to gain some insight into these issues. As the first step of the trial, the rupture process of the Noto Hanto earthquake is inferred from strong motion records, and the distribution of static stress drop is calculated. The results suggest that the causative fault of this earthquake is segmented. The ratio of radiated energy to seismic moment provides a constraint on the activity of the fault system: the causative fault is not very active.

2. Inversion Analysis

Three-component strong motion records of eight stations (inverted triangles in Fig. 1) were used in this analysis. These stations were chosen so that the azimuthal coverage would be as good as possible. The maximum epicentral distance does not exceed 70 km.

The original accelerograms were band-pass filtered between 0.1 and 1 Hz, and numerically integrated twice into displacement. The data length was set to be 30 s from the onset of P-wave for all stations.

The inversion method for analyzing the rupture process is the same as that of Horikawa (2001). An assumed fault plane was divided into small squares called subfaults, and both slip and rupture starting time of each subfault were inferred from observed ground motions with the recursive inversion procedure proposed by Matsu'ura and Hasegawa (1987). Derived solutions depend on the starting models of the recursive procedure. Thus, the equation system from different starting models has to be solved in order to reduce

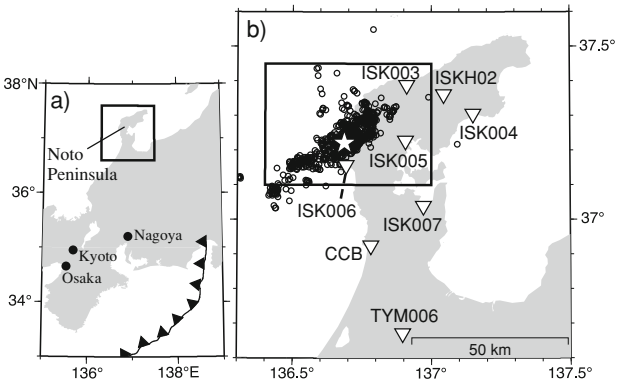

Fig. 1. (a) Map showing the location of the source region of the 2007 Noto Hanto earthquake. The rectangle area corresponds to the source region displayed in panel (b). (b) Map of the source region of the 2007 Noto Hanto earthquake. Aftershocks with $M \geq 2.5$ that occurred by the end of May (about 2 months after the occurrence of the mainshock) are plotted with circles. The epicenter of the mainshock is displayed with a star. The inverted triangles show the stations used in study. The rectangle corresponds to the region shown in Fig. 2.

Table 1. Velocity structure of the basal part.

H	V_P	V_S	ρ	Q_P	Q_S
$4 - H_S$	5.5	3.2	2.6	400	200
20	6.1	3.53	2.7	600	300
16	6.65	3.84	2.8	800	400
∞	8.0	4.62	3.2	1000	500

H: Thickness (km), V_P: P-wave velocity (km/s), V_S: S-wave velocity (km/s), ρ: Density (g/cm^3), H_S: Net thickness of a sedimentary part (km).

Table 2. Velocity structure of sedimentary layers assumed in this study.

ISK003, ISK004, ISK006, ISKH02

H	V_P	V_S	ρ	Q_P	Q_S
0.5	2.8	1.4	2.2	200	100

ISK005

H	V_P	V_S	ρ	Q_P	Q_S
0.02	1.5	0.12	1.7	20	10
0.05	2.1	0.7	2.0	100	50
0.4	2.8	1.4	2.2	200	100

ISK007

H	V_P	V_S	ρ	Q_P	Q_S
0.02	1.5	0.12	1.7	20	10
0.1	1.7	0.4	1.8	60	30
0.4	2.8	1.4	2.2	200	100

CCB

H	V_P	V_S	ρ	Q_P	Q_S
0.7	2.5	1.0	2.0	140	70

TYM006

H	V_P	V_S	ρ	Q_P	Q_S
1.2	2.8	1.4	2.2	200	100

H: Thickness (km), V_P: P-wave velocity (km/s), V_S: S-wave velocity (km/s), ρ: Density (g/cm^3).

the effect of the dependence. The detail of the starting models used in this study will be described later.

The ground-motion contribution from each subfault was expressed with the response of a point source located at the center of the subfault to a horizontally stratified anelastic medium. The point-source response or Green's function was calculated using the reflectivity method by Takeo (1985).

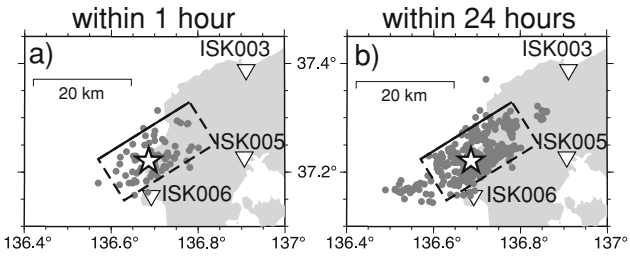

Fig. 2. Aftershock distributions of the 2007 Noto Hanto earthquake and the location of the assumed fault plane (rectangle). Aftershocks are plotted with gray dots. The lower limit of magnitude is the same as that of Fig. 1, but the time range is different. Aftershocks within 1 h after the occurrence of the mainshock are plotted in (a) while aftershocks within 24 h are plotted in (b). Note that the aftershock area clearly expanded during this time period. The bold line stands for the upper edge of the assumed fault plane used in the inversion analysis.

The velocity structures used in this study consisted of a basal part (Table 1) and a sedimentary part (Table 2). The basal velocity structure was assumed to be common for all stations and is the same as the velocity structure adopted in hypocentral determination in the Hokuriku district conducted by Disaster Prevention Research Institute, Kyoto University.

Several velocity structures were assumed for the sedimentary part. These velocity structures were based on geology (Kaseno *et al*., 1992), density structure derived from gravity anomaly (Sutou *et al*., 2004) and borehole logging data if available. After assuming the velocity structures from the above materials, I checked and modified the structures using S-wave codas (Suzuki *et al*., 2005).

3. Fault Parameterization

The 2007 Noto Hanto earthquake was modeled with a single planar fault that had a length of 22 km and a width of 20 km. The upper edge of the fault plane is located at a depth of about 0.7 km. The subfault size was set to be 1×1 km^2. The geometry of the fault plane was fixed to 58° of the strike and 60° of the dip angle. These values were adopted from the moment tensor solutions derived by United States Geological Survey (USGS) and National Institute for Earth Science and Disaster Prevention (NIED). The assumed fault plane covers a 1-h aftershock distribution (Fig. 2). A constant rake angle of 135° was adopted over the fault plane. This value was determined after repeated inversion analysis with different rake angles ranging from 90° to 180°.

As already mentioned, the recursive procedure adopted in this study is sensitive to starting models. In particular, rupture velocity or rupture starting time, which is nonlinearly related to waveforms, strongly controls the solution of the procedure. Thus, rupture velocities from 1.5 km/s to 3.2 km/s were assumed on making starting models.

Combination of various rupture velocities and rake angles yields over 200 starting models, and inversion analysis was performed for all of these starting models. I finally

adopted the inversion result that yielded the least residual.

4. Result of Inversion Analysis

The derived slip distribution is displayed in Fig. 3(a). The average slip is 0.77 m, and the maximum slip reaches 2.7 m. The seismic moment was estimated to be 1.1×10^{19} N m (M_w 6.6). This value of the seismic moment is consistent with the moment tensor solution of USGS (9.1×10^{18} N m) and NIED (1.4×10^{19} N m).

A patch of large (>1.5 m) slip (so-called asperity) includes the hypocenter, extending to a shallow part of the fault plane. A minor asperity was found in a deep and northeastern part. Slip amount between the two asperities is quite small.

A small amount of slip was inferred at the shallow part of the northeastern part located below the Noto peninsula. This feature agrees with the fact that no noticeable surface rupture or deformation associated with the earthquake rupture has been found so far.

Rupture propagation toward the strike direction (northeast) varies place by place, as shown in Fig. 3(b). The rupture mainly propagates to the northeast and in a deeper direction during the first 1 s. The rupture then decelerates between the two asperities from 2 to 3 s. The rupture accelerates after the passage of the zone of small slip. Rupture propagation toward anti-strike direction (southwest) gradually accelerates.

Figure 3(c) shows the seismic moment rate function. The overall feature of the moment rate function is well-approximated with a triangle of duration of about 6 s. The moment rate function reaches a peak value, which corresponds to the rupture of the large asperity close to the hypocenter. The rate function decreases after 2 s, but it begins to increase again at about 4 s. The minor asperity located at a deep and northeastern part of the fault partly contributes to this increase.

The radiated energy estimated from this fault model was 6.1×10^{14} J, where the radiated energy was calculated following Kikuchi and Fukao (1988). The ratio of the radiated energy to seismic moment was estimated to be 5.5×10^{-5}.

Figure 4 shows a comparison of the observed and synthetic waveforms. The observed waveforms are generally well-explained. However, the synthetic waveform of the EW-component of ISK003 fails to reproduce a later phase observed after 18 s. This later phase is commonly observed even in the records for other earthquakes. Hence, I believe that this phase is a locally and secondarily excited surface wave.

We see short-period (~2 s) wave-trains over the entire of the waveforms observed at stations ISK005 and ISK007, which are partly reproduced in the synthetics. Since only a few stations have this character, it is plausible that it is not due to a seismic source but to a velocity structure, especially near-surface or site effect. That is why I have introduced a thin sedimentary layer into the uppermost part of the velocity structure at these stations, as seen in Table 2.

The relative contribution of the two asperities depends on the azimuth from the fault plane (Fig. 5). The major asperity (Asperity 1) generally dominates the synthetics, as seen in the stations ISK006 and CCB. However, the minor asperity (Asperity 2) significantly contributes when a station is located to the east of the fault plane, where the minor asperity is closer to the station than the major one. The observed waveforms at ISK005 and ISK004 are characterized by two impulsive waves. Figure 5 demonstrates that one of the peaks comes from the minor asperity. Since it has been found that the contribution from the minor asperity is significant for multiple stations, the existence of this minor asperity is plausible.

As mentioned before, inversion analysis was performed

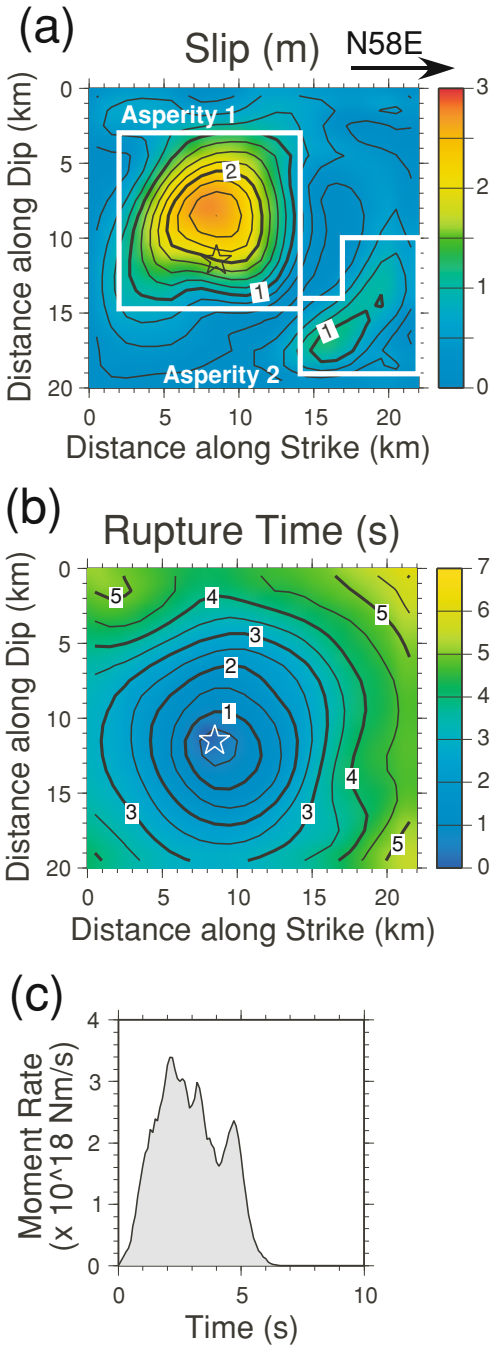

Fig. 3. Fault model of the 2007 Noto Hanto earthquake derived from inversion of strong motion data. (a) Slip distribution. The contour lines start at 0.25 m, and continue at 0.25 m-intervals. (b) Rupture time distribution. The contour lines start at 0.5 s, and continue at 0.5 s-intervals. The stars in the upper two panels stand for the hypocenter. (c) Seismic moment rate function.

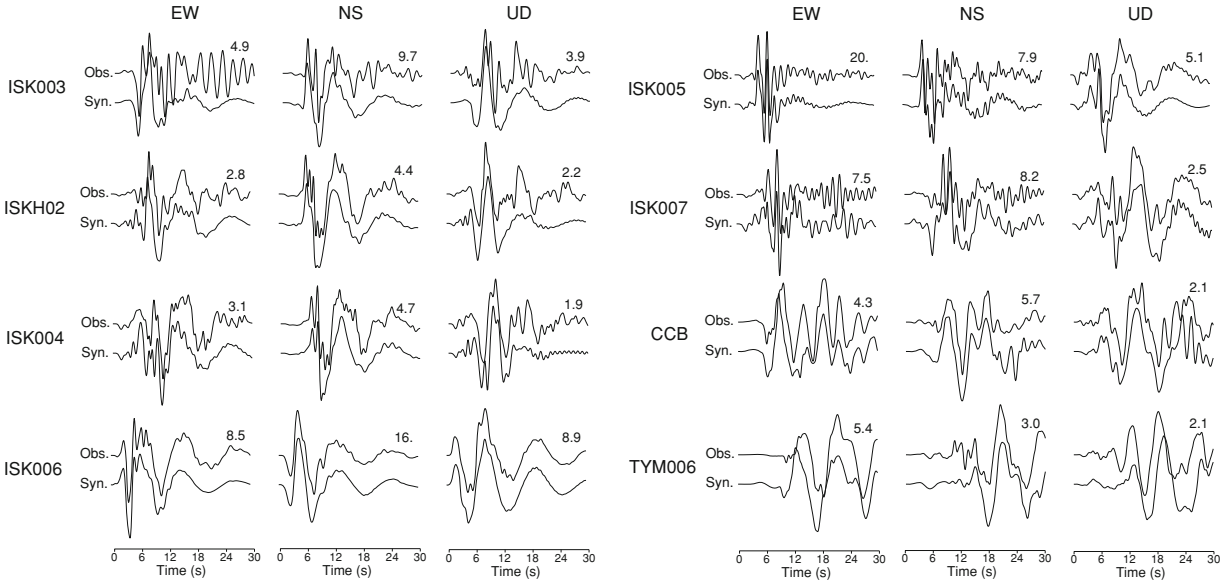

Fig. 4. Comparison of observed (upper) and synthetic (lower) waveforms. The origin of time axis is the arrival of the *P*-wave. The numeral attached to the end of the upper trace stands for peak amplitude of the observed waveform in centimeter.

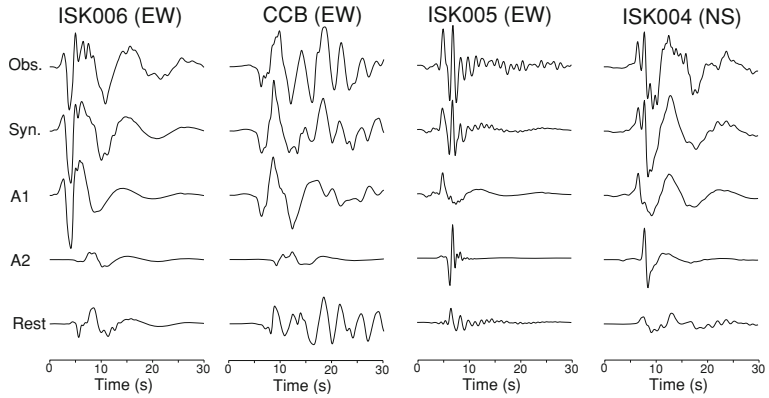

Fig. 5. An example of a comparison of data (top trace) and synthetics (second trace) with contributions to the synthetics from Asperity 1 (third trace), Asperity 2 (fourth trace), and the rest of the fault plane (bottom trace). The region of asperities is defined in Fig. 3. The station code and component are shown above each observed waveform.

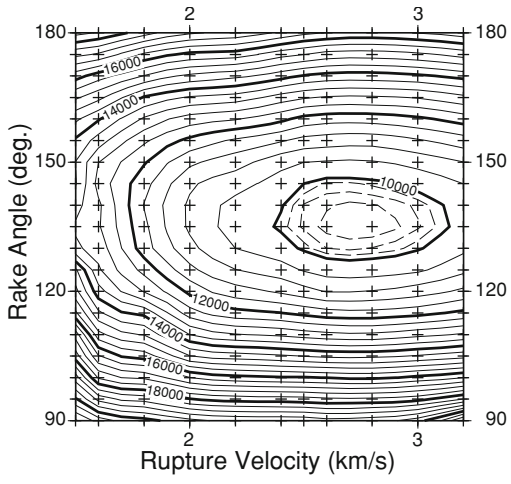

Fig. 6. Contour map of residuals. Crosses show the assumed values as starting model. Solid contours are drawn at 400 intervals. Residuals below 10000 (dashed contours) are plotted at 100 intervals to show the location of the least residual clearly.

for various rupture velocities and rake angles. The residuals of all trials are shown in a contour map (Fig. 6). The moment tensor solution of USGS has a rake angle of 114° and a dominant component of dip-slip. The contour map shows that such a mechanism is not plausible because the rake angle yielded larger residuals than other angles.

We see no local minimum on the contour map. This suggests that the nonlinearlity of the equation system solved in this study is not strong and therefore validates the use of the recursive procedure, where weak nonlinearity is assumed.

5. Static Stress Drop

We calculated the distribution of static stress drop with the analytic formula of Okada (1992), showing the result in Fig. 7. The maximum value of static stress drop is over 16 MPa and still appears on the major asperity.

Existence of the minor asperity is more clearly seen on the distribution of static stress drop. The maximum value of stress drop is beyond 12 MPa for the minor asperity. The difference between the maximum values is over twice for

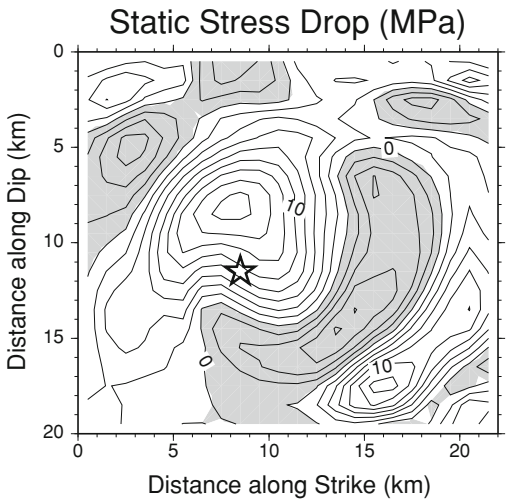

Fig. 7. Distribution of static stress drop along slip direction. The contour interval is 2 MPa. In gray regions, static stress drop is negative. The star stands for the hypocenter.

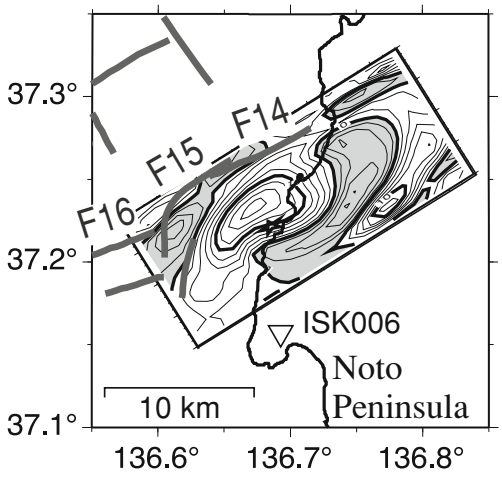

Fig. 8. Distribution of static stress drop projected onto the ground surface. Dark gray lines stand for surface faults identified by Katagawa *et al.* (2005).

slip amount, but the difference is only 1.3 times and almost comparative for static stress drop.

Areas with small slip correspond to those of negative stress drop for this earthquake. As mentioned, the rupture propagated faster toward the northeast and deeper direction during the first 1 s. It should be noted that the fast propagation ceased when the rupture front met the zone of negative stress drop. Moreover, the slow rupture propagation during the first 3–4 s appeared when the rupture propagated within the zone. These characters mean that the zone of negative stress drop acted as a barrier and segment boundary.

6. Discussion

I have shown that two asperities with comparative static stress drop are located on the fault plane and estimated the peak values to be 12–16 MPa. Horikawa (2001) estimated a peak value of about 4 MPa for the 1997 Kagoshima doublet (M_w 6.0, 5.9), and Horikawa (2006) estimated the peak value to be about 12 MPa for the 2005 West Off Fukuoka Prefecture earthquake (M_w 6.4). Miyatake (1992) analyzed four Japanese intraplate earthquakes—the 1969 Gifu earthquake (M 6.6), the 1974 Izu-Hanto-Oki earthquake (M 6.9), the 1980 Izu-Hanto-Toho-Oki earthquake (M 6.7) and the 1984 Western Nagano earthquake (M 6.8)—and shown that peak values of the stress drop range from 8 to 18 MPa. Taking these results into consideration, I conclude that the peak value of the Noto Hanto earthquake is slightly high but within the variation of the previous results.

The causative fault of the 2007 Noto Hanto earthquake likely corresponds to the F14 and F15 faults in Katagawa *et al.*'s (2005) classification (Fig. 8). The southwestern edge of the main asperity correlates well with the boundary between the F15 and the F16. This suggests that the fault boundary identified from shallow (<0.4 km) seismic surveys (Katagawa *et al.*, 2005) can approximately extend downward into the seismogenic layer.

I have shown that an area of negative stress drop is located between the two asperities. The area of negative asperity is located near the western coast of the Noto peninsula (Fig. 8). If the segmentation of surface faults corresponds to the fault configuration in depth at the northeastern edge of the F14, the northeastern boundary will appear around the coast line, and the F14 does not extend to the peninsula. This means that the length of the F14 is about 10 km and similar to those of other faults. In this sense, the F14 is not exceptional in the Katagawa *et al.*'s classification.

It may seem strange that the boundary between the F14 and the F15 appeared just above the major asperity (Fig. 8), but we should note that the distribution of static stress drop at the upper 2–3 km of the causative fault seems to correlate with the configuration of the surface faults. That is, the boundary between the F14 and the F15 is located above the area of negative stress drop. A fault boundary identified on the surface is often assumed to extend vertically downward to the bottom of a seismogenic layer, but this earthquake illustrates that validity of the assumption should be carefully examined.

The ratio of radiated energy to seismic moment is correlated with slip rate or repeat times of faults (Kanamori, 1994), and this ratio will be useful for estimating the repeat times of the fault. I will compare the 2007 Noto Hanto earthquake with the 1995 Kobe earthquake (M_w 6.8) and the 2000 Tottori earthquake (M_w 6.6).

Ide (2002) used several fault models and estimated the ratio of the 1995 Kobe earthquake to be $1.1–1.7\times10^{-5}$. For the 2000 Tottori earthquake, Jin and Fukuyama (2005) estimated the ratio to be 3.6×10^{-5} directly from ground motion spectra without constructing a fault model. Ide (2002) pointed out that the ratio derived from spectra is systematically about three times larger than that derived from a fault model. Thus, the ratio estimated by Jin and Fukuyama (2005) was divided by three for direct comparison, and the resultant value of 1.2×10^{-5} was adopted for the 2000 Tottori earthquake. In summary, the two earthquakes have a similar value of $\sim 1 \times 10^{-5}$ for the ratio of radiated energy to seismic moment, and the ratios are a fraction (about 20%) of that of the 2007 Noto Hanto earthquake.

It is possible to estimate repeat times of these two earthquakes. However, the estimation is not straightforward for

the Kobe earthquake because the causative faults of the earthquake have different repeat times of 400 years and 1700–2000 years according to trench surveys (e.g. Awata and Suzuki, 1996). Although the difference between the two values is not small, I will tentatively take the average value of 1000 years as repeat times. The repeat times of the Tottori earthquake can be estimated to be 750–1200 years from the recent event revealed by a trenching study (Inoue *et al*., 2002). Comparison of the 2007 Noto Hanto earthquake with these two earthquakes suggests that the 2007 Noto Hanto earthquake has repeat times longer than 1000 years when taking into consideration that the repeat times become shorter as the ratio decreases (Kanamori, 1994). The estimated repeat times mean that the causative fault of the 2007 Noto Hanto earthquake is not very active. In future studies, it will be important to constrain the upper value of the slip rate with a validation of the estimation in this study for evaluation of seismic potential in this region.

Acknowledgments. I am grateful to the National Institute for Earth Science and Disaster Prevention (NIED) for providing strong ground motions recorded with K-NET (Kinoshita, 1998) and KiK-net (Aoi *et al*., 2000). The strong motion data recorded at the station CCB was provided by Japan Meteorological Agency (JMA). Minoru Takeo allowed me to use his computer code of the reflectivity method. Comments by Yasumaro Kakehi and Yoshihiro Hiramatsu are greatly appreciated. The hypocenters determined and provided by JMA are based on stations of the following universities and institutes: Hokkaido University, Hirosaki University, Tohoku University, the University of Tokyo, Nagoya University, Kyoto University, Kochi University, Kyushu University, Kagoshima University, JMA, NIED, Japan Marine Science and Technology Center, and National Institute of Advanced Industrial Science and Technology. Figures were prepared with the Generic Mapping Tools (Wessel and Smith, 1998).

References

Aoi, S., K. Obara, S. Hori, K. Kasahara, and Y. Okada, New strong-motion observation network: KiK-net, *Eos*, **81**, F863, 2000.

Awata, Y. and Y. Suzuki, Paleoseismology and activeity study of the Nojima fault system, which generated the Hyogo-ken Nanbu earthquake of Jannuary 17, 1995, *Open-File Rep. Geol. Surv. Jap*., **259**, 1–5, 1996 (in Japanese).

Horikawa, H., Earthquake doublet in Kagoshima, Japan: Rupture of asperities in a stress shadow, *Bull. Seismol. Soc. Am*., **91**, 112–127, 2001.

Horikawa, H., Rupture process of the 2005 West Off Fukuoka Prefecture, Japan, earthquake, *Earth Planets Space*, **58**, 87–92, 2006.

Ide, S., Estimation of radiated energy of finite-source earthquake models, *Bull. Seismol. Soc. Am*., **92**, 2994–3005, 2002.

Inoue, D., K. Miyakoshi, K. Ueta, A. Miyawaki, and K. Matsuura, Active fault study in the 2000 Tottori-ken Seibu earthquake area, *Zisin Ser. 2*, **54**, 557–573, 2002 (in Japanese with English abstract).

Jin, A. and E. Fukuyama, Seismic energy for shallow earthquakes in southwest Japan, *Bull. Seismol. Soc. Am*., **95**, 1314–1333, 2005.

Kanamori, H., Mechanics of earthquakes, *Ann. Rev. Earth Planet. Sci*., **22**, 207–237, 1994.

Kaseno, Y., S. Miura, and S. Fujii, Hills and plains in the Hokuriku District, Japan, *Urban Kubota*, **31**, 64 pp., 1992 (in Japanese).

Katagawa, H., M. Hamada, S. Yoshida, H. Kadosawa, A. Mitsuhashi, Y. Kono, and Y. Kinugasa, Geological development of the west sea area of the Noto peninsula district in the Neogene Tertiary to Quatrernary, central Japan, *J. Geogr.*, **114**, 791–810, 2005 (in Japanese with English abstract).

Kikuchi, M. and Y. Fukao, Seismic wave energy inferred from long-period body wave inversion, *Bull. Seismol. Soc. Am*., **78**, 1707–1724, 1988.

Kinoshita, S., Kyoshin net (K-NET), *Seismol. Res. Lett*., **69**, 309–332, 1998.

Matsu'ura, M. and Y. Hasegawa, A maximum likelihood approach to nonlinear inversion under constraints, *Phys. Earth Planet. Inter.*, **47**, 179–187, 1987.

Miyatake, T., Dynamic rupture processes of inland earthquakes in Japan weak and strong asperities, *Geophys. Res. Lett*., **19**, 1041–1044, 1992.

Okada, Y., Internal deformation due to shear and tensile faults in a half-space, *Bull. Seismol. Soc. Am*., **82**, 1018–1040, 1992.

Ota, Y., T. Matsuda, and K. Hirakawa, Active faults in Noto peninsula, Central Japan, *Quat. Res*., **15**, 109–128, 1976 (in Japanese with English abstract).

Sutou, H., Y. Kitaguchi, K. Yamamoto, and Y. Kono, Gravity anomaly and basement structures in southern part of the Noto peninsula, Japan—Relationship among gravity anomaly, active faults and seismicity—, *Zisin Ser. 2*, **56**, 363–377, 2004 (in Japanese with English abstract).

Suzuki, H., M. Morino, K. Iwamoto, Y. Liu, H. Fujiwara, and Y. Hayakawa, 3D subsurface structural model for strong motion simulation around Lake Biwa, Southwest Japan, *Zisin Ser. 2*, **58**, 91–106, 2005 (in Japanese with English abstract).

Takeo, M., Near-field synthetic seismograms taking into account of the effects of anelasticity—The effects of anelastic attenuation on seismograms caused by a sedimentary layer—, *Meteorol. Geophys*., **36**, 245–257, 1985 (in Japanese with English abstract).

Usami, T., *Materials for comprehensive list of destructive earthquakes in Japan, [416]-2001*, 605 pp., University of Tokyo Press, Tokyo, 2003 (in Japanese).

Wessel, P. and W. H. F. Smith, New, improved version of Generic Mapping Tools released, *Eos*, **79**, 579, 1998.

H. Horikawa (e-mail: h.horikawa@aist.go.jp)